

A Multiscale Approach to the Mixed Lubrication Regime: Application to Mechanical Seals

André Parfait Nyemeck · Noël Brunetière · Bernard Tournier

Received: 26 March 2012 / Accepted: 15 June 2012 / Published online: 29 June 2012
© Springer Science+Business Media, LLC 2012

Abstract This paper presents a multiscale approach to solve the problem of mixed lubrication in mechanical seals. In fact, the lubricating fluid film developed between the faces of mechanical seals is usually a fraction of a micron in thickness, leading to a mixed lubrication regime. However, over a velocity threshold the fluid film can completely separate the faces because of the hydrodynamic effect due to the surface roughness, even if the surfaces are nominally parallel. To study this phenomenon, a deterministic model is preferable because the stochastic theory based on flow factors is unable to reproduce this effect. Unfortunately, a deterministic approach needs a prohibitive amount of nodes and computation time. This is why a multiscale model is proposed. It is composed of a micro-deterministic model working on a small area coupled with a macro model giving the pressure distribution on a macro-mesh. The results of the multiscale model are compared to those of a pure deterministic model in terms of accuracy and computation time when the area of the macro-cells is varied.

Keywords Computational and math methods for tribology · Fluid mechanics methods · Roughness effects in hydrodynamics · Surface roughness · Face seals · Mechanical seals

List of Symbols

Variables

| | |
|----------------------|--|
| a | Major axis of elliptical contact area (m) |
| b | Minor axis of elliptical contact area (m) |
| B_h | Balance ratio |
| C_f | Friction torque (N m) |
| C_{f_2} | Dry friction torque (N m) |
| d | Diameter (m) |
| D | Universal variable |
| E | Young's modulus (Pa) |
| F | Switch function |
| F_c | Contact force in the summit of asperity (N) |
| F_{closing} | Closing force (N) |
| F_{opening} | Opening force (N) |
| h | Film thickness (m) |
| h_0 | Mean film thickness (m) |
| Ku | Kurtosis coefficient |
| N_r | Number of nodes in the radial direction |
| N_θ | Number of nodes in the circumferential direction |
| N_{bl} | Number of macro-cells |
| p | Pressure in the film (Pa) |
| p_c | Pressure in the contact area (pa) |
| p_i | Pressure imposed at the boundary of macro-cells (Pa) |
| p_{cav} | Cavitation pressure (Pa) |
| $q^{(\cdot)}$ | Flow rate (kg/s) |
| R | Radius (m) |
| (r_r, r_θ) | Curvature radii at the summit of asperity (m) |
| R_h | Hydraulic radius (m) |
| Sk | Skewness coefficient |
| Sq | Roughness standard deviation (m) |
| S_u | Source term |
| W | Force (N) |
| W_h | Hydrodynamic lift (N) |

A. P. Nyemeck · N. Brunetière (✉) · B. Tournier
Département GMSC, Institut P' CNRS-Université de Poitiers-
ENSMA UPR 3346, BP 30179, SP2MI-Téléport 2, Boulevard
Marie et Pierre Curie, 86962 Futuroscope Chasseneuil Cedex,
France
e-mail: noel.brunetiere@univ-poitiers.fr

| | |
|------------|---|
| W_{hs} | Hydrostatic lift (N) |
| W_t | Total load (N) |
| z | Height distribution of the simulated surfaces (m) |
| Γ | Curvature difference |
| Δp | Macro-pressure variation (Pa) |
| μ | Fluid viscosity (Pa s) |
| ρ | Fluid density (kg/m ³) |
| ν | Poisson's ratio |
| δ | Interference (m) |
| ω | Rotation speed (rpm) |

Dimensionless Parameter

| | |
|-----|--|
| f | Friction coefficient $\frac{2Cf}{(R_o+R_i)F_{closing}}$ |
| G | Duty parameter $\frac{\mu\omega(R_o^2-R_i^2)}{2F_{closing}}$ |

Index

| | |
|--------|-------------|
| 1 | Stator |
| 2 | Rotor |
| i, j | Array index |
| eq | Equivalent |
| o | Outer |
| i | Inner |
| ref | Referential |

1 Introduction

Mechanical seals are a kind of sealing component for rotating shafts. They are basically composed of two flat rings (rotor and stator) maintained in close contact and constituting the sealing dam between the pressurised fluid and the atmosphere. In spite of the fact that the two rings are initially in contact, they are generally separated by a very thin fluid film during operation. Indeed, in some experimental investigations [1], it has been shown that during operation, mechanical seals exhibit a Stribeck curve (the friction coefficient versus the duty parameter G) typical of the transition from mixed lubrication to full hydrodynamic lubrication regimes. Therefore, the seal performance depends on the surface roughness that will affect the lubrication process as well as the contact between asperities. The mixed lubrication can be modelled by two different methods:

1.1 Stochastic modelling

This method uses selected statistical parameters to deal with the influence of roughness on lubrication. Tzeng and Saibel [2] and then Christensen [3] developed this concept in the case of one-dimensional roughness. Patir and Cheng [4, 5] proposed a new theory able to deal with all types of roughness. They introduced flow factors, which indicate the effect of roughness on the flow, in the Reynolds

equation. This method has been widely used in lubrication but is unfortunately unable to reproduce the hydrodynamic lift with nominally parallel surfaces configuration as in mechanical seals.

1.2 Deterministic modelling

The principle of deterministic modelling consists in representing as accurately as possible the surface topography and solving the usual Reynolds equation with this fine surface description. This type of approach needs a very fine mesh and was first used in line or point contacts that have a small area extent [6–8]. More recently, Dobrica et al. [9] presented some results for partial bearing having a more extended lubricated interface. The case of nominally flat surfaces was studied by Minet et al. [10], who presented a model of mixed lubrication for mechanical seals. They showed that surface roughness is able to generate a hydrodynamic lift-off leading to a full hydrodynamic lubrication regime above a velocity threshold. This hydrodynamic load generation is correlated to the appearance of micro-cavitation as experimentally observed by Hamilton et al. [11].

However, the main drawback of deterministic approaches is the tremendous amount of computer memory and central processing unit (CPU) time required, which could exceed modern computing resources limits when real surface areas are considered. In the literature, different techniques have been developed for similar problems, but the general idea behind all these methods is the multiscale treatment. The main goal of this approach is to obtain the macroscopic scale solution both accurately and efficiently, while including the effect of the micro-scale (e.g. the roughness effect).

The literature on multiscale methods is very large, and we focused our attention on the numerical models developed for flow in porous media where the average flow depends on the local micro-scale permeability distribution. Hou and Wu [12] were among the first to propose a multiscale finite element method followed by Jenny et al. [13] with the multiscale finite volume method. These methods are based on the construction of special element base functions that are adaptive to the local property of the problem. The coefficients of these functions are determined by solving a micro-scale problem. These solutions are generally globally but not locally mass-conserving.

This paper presents a multiscale model for the numerical calculation of the pressure distribution. The principle of this approach is to express pressure on a macro-mesh by using a mass-conservative law whose coefficients are computed on a micro-scale mesh. The results are then compared to the ones obtained with the pure deterministic model of Minet et al. [10].

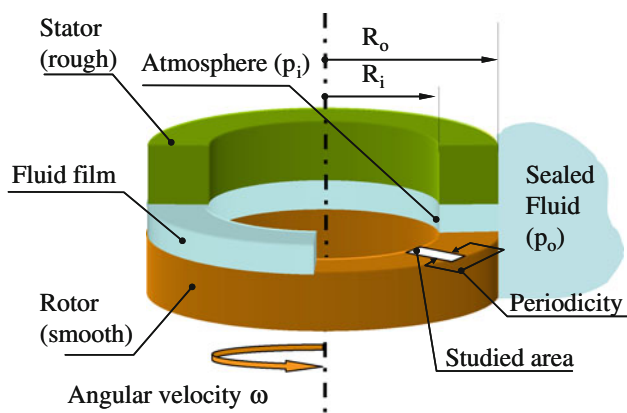


Fig. 1 Mechanical seal configuration

2 Theoretical Considerations

A typical face seal configuration is presented in Fig. 1. For this study, the rotor is considered to be smooth, whereas the stator is rough. The nominal surfaces are flat and parallel. The study is performed on a small radial band of the seal interface, as shown in Fig. 1.

2.1 Micro-scale Fluid Model Description

Minet et al. [10] presented a model of mixed lubrication in mechanical seals based on a deterministic approach. This approach uses very fine and regular meshes in the investigated area. In addition to the usual fluid film lubrication assumptions, the following additional hypotheses were used:

- The problem is stationary and isothermal,
- Periodic conditions are imposed at the circumferential boundaries,
- Pressure is imposed at the radial boundaries (inner and outer radii of the sub-domain)

The lubricant flow was modelled by using the finite volume method. The flow rates resulting from the pressure distribution and the faces displacement must vanish in each considered mesh element. Thus, the obtained mass flow balance in a micro-cell (Fig. 2) can be written as follows:

$$q_W^{(r)} + q_S^{(r)} - q_E^{(\theta)} - q_N^{(\theta)} = 0. \tag{1}$$

The expression of the mass flow is

$$\begin{cases} q_w^{(r)} = -\frac{h_w^3}{12\mu} R_w \Delta\theta \frac{\partial}{\partial r} (FD)_w \\ q_e^{(\theta)} = -\frac{h_e^3}{12\mu} R_e \Delta\theta \frac{\partial}{\partial r} (FD)_e \\ q_n^{(\theta)} = -\frac{h_n^3}{12\mu} \frac{\Delta R}{R_n \Delta\theta} \frac{\partial}{\partial \theta} (FD)_n + 0.5 h_n \Delta R R_n \omega [1 - D_P (1 - F_n)] \\ q_s^{(r)} = -\frac{h_s^3}{12\mu} \frac{\Delta R}{R_s \Delta\theta} \frac{\partial}{\partial \theta} (FD)_s + 0.5 h_s \Delta R R_s \omega [1 - D_S (1 - F_s)] \end{cases} \tag{2}$$

In Eq. (2), h represents the local film thickness, μ the fluid viscosity, and ΔR and $\Delta\theta$ are the sampling interval of the mesh. Each derivative is approximated by a first-order finite difference:

$$\begin{cases} \frac{\partial}{\partial r} (FD)_w \approx \frac{F_P D_P - F_W D_W}{\Delta R}; & \frac{\partial}{\partial \theta} (FD)_s \approx \frac{F_P D_P - F_S D_S}{\Delta\theta} \\ \frac{\partial}{\partial r} (FD)_e \approx \frac{F_E D_E - F_P D_P}{\Delta R}; & \frac{\partial}{\partial \theta} (FD)_n \approx \frac{F_N D_N - F_P D_P}{\Delta\theta} \end{cases} \tag{3}$$

In this expression, F is a switch function, and D a universal variable which can represent the pressure p or the fluid density ρ depending on whether the cell is cavitated or active:

$$\begin{aligned} F = 0 & \quad D = \frac{\rho}{\rho_0} - 1 \quad p = p_{cav} \\ F = 1 & \quad D = p - p_{cav} \quad \rho = \rho_0. \end{aligned} \tag{4}$$

By reporting expressions (2, 3) in Eq. (1), the following expression is derived:

$$A_P D_P + A_N D_N + A_S D_S + A_W D_W + A_E D_E + S_u = 0. \tag{5}$$

The micro-pressure distribution is obtained by solving Eq. (5) numerically on a fine mesh, by means of a fast LU

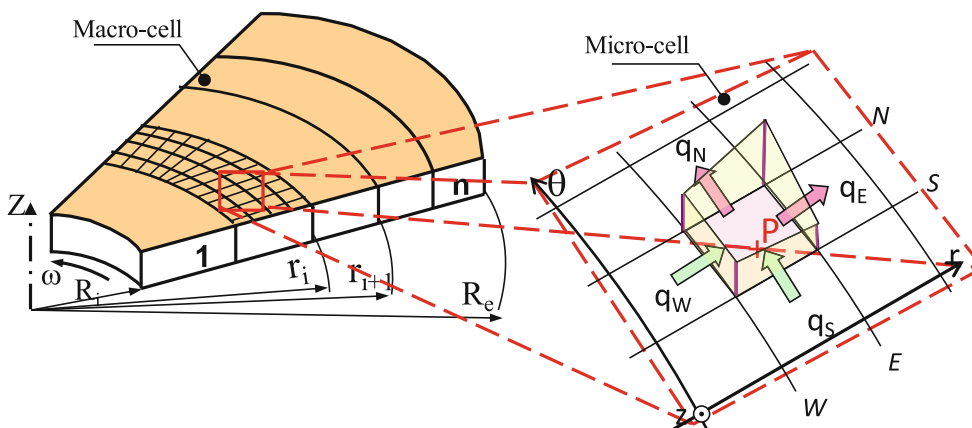


Fig. 2 Typical investigated area with micro and macro-scale description

decomposition technique for sparse matrices. This model will be used here to obtain pressure field at the micro-scale.

2.2 Macro-scale Fluid Model Description

The macro-scale mesh is obtained by subdividing the studied area into a number of macro-cells in the radial direction, as illustrated in Fig. 2. The aim of this model is to determine the macro-pressure at the boundaries of each macro-cell. The macro configuration is assumed to be axisymmetric and the macro-pressure is thus a radial distribution. This is the main simplification induced by this multiscale model: the microscopic pressure distribution is assumed to be constant in the circumferential direction at each macro-cell boundary. The effect of this assumption on the accuracy of the solution will be analysed in the following sections of the paper. The radial flow rate across macro-cells can be expressed as a nonlinear function of the pressure applied at the cell boundaries, i.e.

$$q_r^{(i)} = q_r^{(i)}(p_i, p_{i+1}), \tag{6}$$

where $q_r^{(i)}$ is the radial flow rate in the macro-cell number i . Equation (6) can be further developed by using a first-order Taylor transformation. Therefore, the flow rate approximation $q_r^{(i)}$ is given as follows:

$$q_r^{(i)}(p_i + \Delta p_i, p_{i+1} + \Delta p_{i+1}) \cong q_r^{(i)}(p_i, p_{i+1}) + a^{(i)} \Delta p_i + b^{(i)} \Delta p_{i+1} + o(\Delta p^2), \tag{7}$$

where a and b are first-order derivatives:

$$a^{(i)} = \frac{\partial q_r^{(i)}}{\partial p_i} \tag{8}$$

$$b^{(i)} = \frac{\partial q_r^{(i)}}{\partial p_{i+1}}.$$

These three coefficients ($a^{(i)}$, $b^{(i)}$ and $q_r(p_i, p_{i+1})$) are computed with the micro-scale model for each macro-cell. q_r is the mass flow obtained when a given pressure differential is applied at the boundaries of the macro-mesh, whereas a and b are obtained by applying a small pressure variation at, respectively, inner and outer radii. They can be calculated independently for each macro-cell and determined through parallel computation. When the coefficients are known for all the macro-cells, it is possible to compute a radial macro-pressure distribution that ensures the mass flow rate conservation between contiguous macro-cells:

$$q_r^{(i)} - q_r^{(i+1)} = 0 \tag{9}$$

giving thus:

$$a^{(i)} \Delta p_i + [b^{(i)} - a^{(i+1)}] \Delta p_{i+1} - b^{(i+1)} \Delta p_{i+2} + q_r^{(i)}(p_i, p_{i+1}) - q_r^{(i+1)}(p_{i+1}, p_{i+2}) = 0, \tag{10}$$

where Δp are the unknown pressure variations leading to mass conservation. Since Eq. (10) is nonlinear, the process should be repeated until convergence is reached on the macro-pressure distribution.

2.3 Constitutive Model for Asperity Contact

The contact between the smooth rotor and rough stator first took place at the highest asperity points. The contact loads are weak and the rings are generally obtained from brittle elastic materials. They cannot undergo plastic deformation. Moreover, it is assumed that only the normal component of the contact stress supported by the asperities contributes to their deformations. The tangential component is considered by means of a friction coefficient.

The rough surface topography being known, the peaks of the asperities, which are the local maxima of the roughness height (Fig. 3), are identified. The curvature radii of the summits can be calculated from the neighbour nodes' height distribution. The dimensions of the contact areas are assumed to be small compared to the radii of the asperities because of the light loads supported by the seal interface.

The contact model presented herein adheres to the one developed by Hamrock and Dowson [14]. It described an elliptic and planar contact. Thereby, the maximal elastic pressure in ellipsoidal contact is defined as follows:

$$p_c = \frac{3}{2} \frac{F_c}{\pi ab}, \tag{11}$$

where F_c is the contact load, a and b , the respective major and minor semi-axis of the contact ellipse. The relation between a and b is defined by the elliptic parameter of contact, i.e. $k = a/b$. The contact load F_c is related to the interference δ through the following relation:

$$F_c = \pi k E_{eq} \left[\frac{2 E_{req}}{9} \left(\frac{\delta}{F} \right)^3 \right]^{\frac{1}{2}}, \tag{12}$$

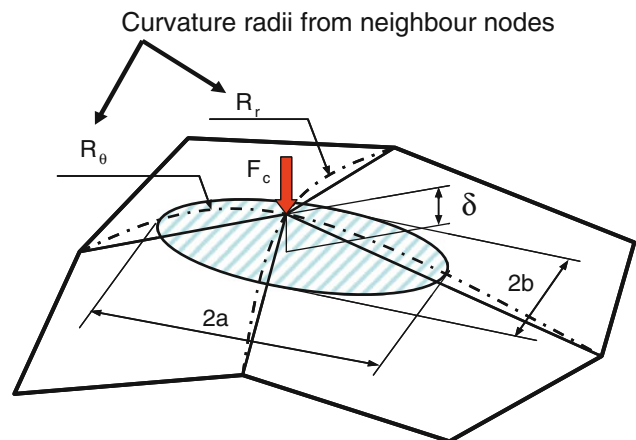


Fig. 3 Contact characteristics of an asperity

where E_{eq} is the equivalent Young’s modulus, and E and F are the elliptic integrals of the first and second kinds, respectively [15].

2.4 The Equilibrium Condition

The opening force consists of the pressure force in the fluid film and total contact force due to asperity contacts. It is expressed as:

$$F_{opening} = W_t + W_h, \tag{13}$$

where W_t and W_h are, respectively, the total contact force and the fluid force on all the N_{bl} macro-cells:

$$W_t = \frac{2\pi}{\theta_t} \sum_{i=1}^{nbl} W_t^{(i)} = \frac{2\pi}{\theta_t} \sum_{i=1}^{nbl} \sum_{nc(i)} W_c^{(i)} \tag{14}$$

$$W_h = \frac{2\pi}{\theta_t} \sum_{i=1}^{nbl} W_h^{(i)} = \frac{2\pi}{\theta_t} \sum_{i=1}^{nbl} \int_{r_i}^{r_{i+1}} \int_0^{\theta_t} p r dr d\theta.$$

Furthermore, the force that is supposed to balance the opening force and maintain the seal surfaces as close as possible is due to the action of the pressure of the sealed

fluid on the back side of the floating ring. It is called the closing force, and it is defined as:

$$F_{closing} = \pi(R_o^2 - R_h^2)p_o + \pi(R_h^2 - R_i^2)p_i, \tag{15}$$

where R_h is the hydraulic radius. It allows the balance ratio B_h of the seal to be defined as:

$$B_h = \frac{R_o^2 - R_h^2}{R_o^2 - R_i^2}. \tag{16}$$

The average distance between the rings is adjusted by a Newton algorithm, so that the hydrodynamic lift and the contact force balance the closing force applied on the floating ring.

3 General Solution Procedure

The flowchart shown in Fig. 4 depicts the overall procedure and the way the solution is checked for convergence. The computation starts with the initial input including: the surface topography, the material properties, and the operating and design parameters. Afterwards, the overall micro-mesh

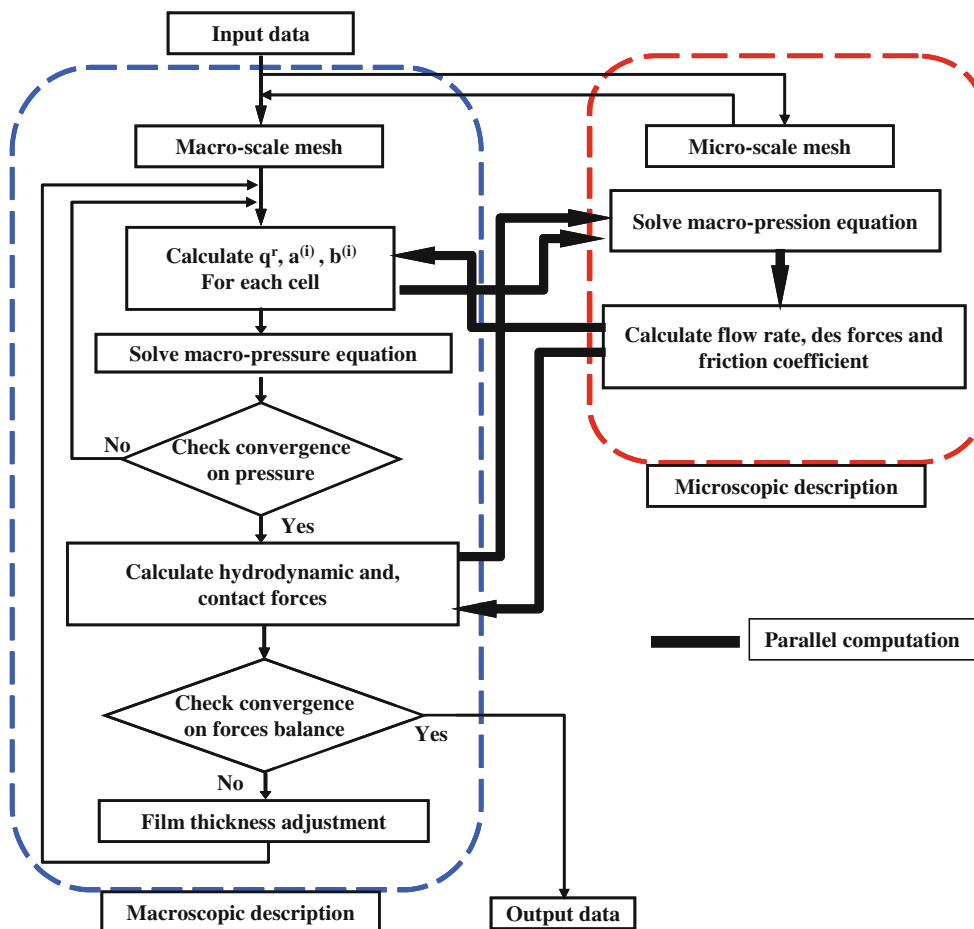


Fig. 4 Flowchart describing the multiscale solution procedure

is divided into a given number N_{bl} of macro-cells. This step is followed by an iterative procedure, where the coefficients q_r , a and b are calculated for each macro-cell. These coefficients are evaluated with the micro-scale model, where the micro-pressure and flow rate are calculated using the finite volume method and a fast LU matrix decomposition technique. The macro-pressure distribution is computed by solving the tri-diagonal system given by Eq. (6). The process is repeated until the macro-pressure field is converged, meaning that the average variation of p is lower than 10^{-6} times the average p value. The nonlinearity arises from the micro-cavitation occurring within each macro-element. Next, the forces are

calculated and the opening force is compared with the closing force. If the forces are not balanced, the film thickness is further adjusted via the Newton algorithm until the final solution achieves convergence. The convergence criterion on the relative force error was set at 10^{-5} .

Since the coefficients q_r , a and b can be calculated independently for each macro-cell, the numerical algorithm can easily be parallelized. The Open MP library is used to distribute the work on the different processors of the computer. This approach is very efficient to reduce computation time. The parallel computations zones are indicated by a thick line in Fig. 4.

Table 1 Operating and design parameters of the mechanical seal

| | |
|----------------------------------|-------------------------|
| Inner radius, R_i | 0.029 m |
| Outer radius, R_o | 0.033 m |
| Balance ratio | 0.75 |
| Rotation speed, ω | 10–1,000 rad/s |
| Outer pressure, p_o | 1 Mpa |
| Inner pressure | 0 |
| Fluid viscosity, μ | 10^{-3} Pa s |
| Fluid density, ρ_o | 1,000 kg/m ³ |
| Cavitation pressure, p_{cav} | −0.01 MPa |
| Dry contact friction coefficient | 0.2 |
| Stator material | Silicon carbide |
| Rotor material | Carbon |

4 Results and Discussion

As noted herein, the possibility of reducing the computation time is one of the main driving factors for using the multiscale approach to model mixed lubrication in face seals. The mechanical seal characteristics used in the numerical analysis are presented in Table 1.

The rough surfaces (Figs. 5, 6) used in the algorithm were generated numerically [15] and their characteristics are shown in Table 2. The surfaces are non-Gaussian because of the polishing process and the running-in of the seals. Moreover, they are periodical in the circumferential direction, to be in line with the assumptions of the model.

Fig. 5 Top view and lateral view of surface 1

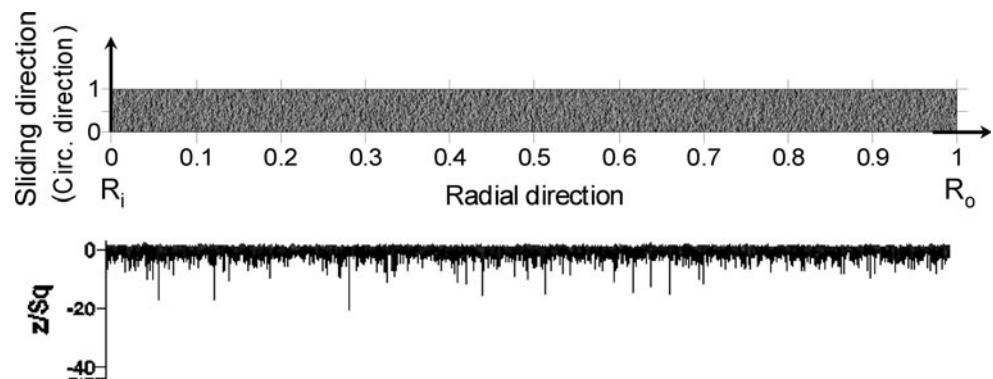


Fig. 6 Top view and lateral view of surface 2

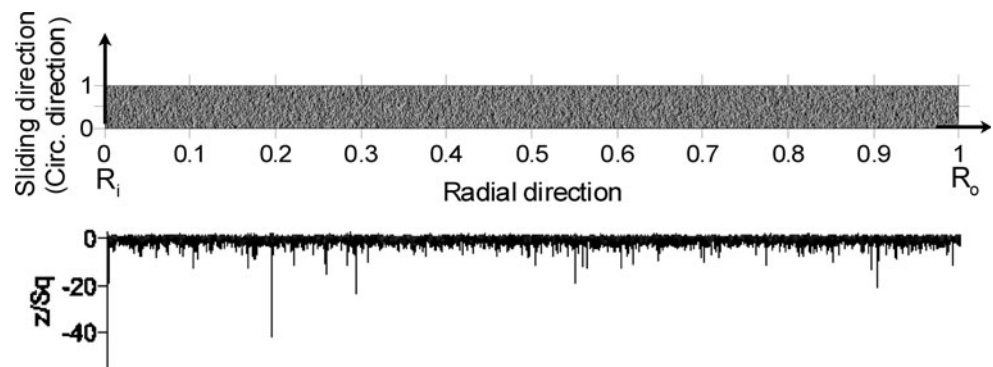


Table 2 Characteristics of the rough surface and of the mesh

| | Surface 1 | Surface 2 |
|--|-------------------|-----------|
| Roughness standard deviation, Sq | 0.1 μm | |
| Skewness coefficient, Sk | -2.7 | -3 |
| Kurtosis coefficient, Ku | 35.4 | 58 |
| Number of cells in radial dir. | 4,000 | |
| Number of cells in circ. dir. | 200 | |
| Radial correlation length at 80 % (μm) | 8 | |
| Circumference correlation length at 80 % (μm) | 10 | |

In the studied case, 4,000 nodes in the radial direction, and 200 in the circumferential direction are considered well suited and efficient [10].

4.1 Model Validation

The results from the present multiscale solution are compared with the pure deterministic model of Minet et al. [10]. The objective is not to analyse the physical significance of the results, but to study the performance of the multiscale approach compared to a deterministic method. For convenience, the results are presented as a function of the duty parameter G , which controls the magnitude of the hydrodynamic effect in the fluid film:

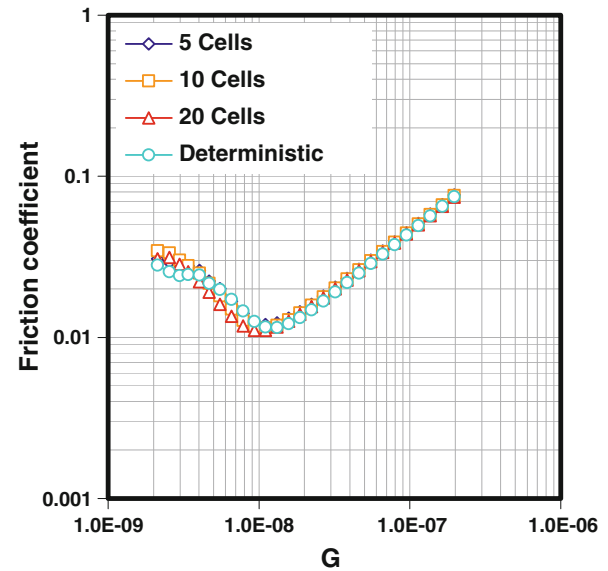
$$G = \frac{\mu\omega(R_o^2 - R_i^2)}{2F_{\text{closing}}} \tag{17}$$

In this section, the number of macro-cells is varied from five, which is expected to give a more accurate solution, to 20 which is expected to give a faster solution (reduced computation time).

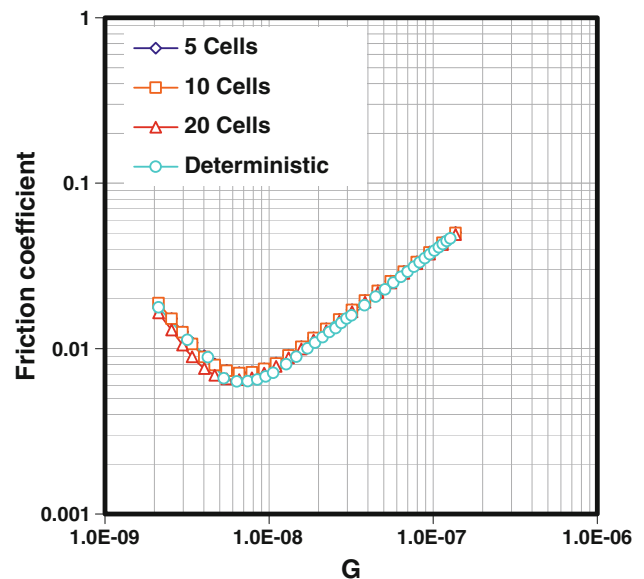
The Stribeck curve is an overall view of the friction variation for the entire range of the lubrication regimes, including the hydrodynamic and mixed lubrication regimes. Figure 7a, b presents the Stribeck curves that were numerically obtained for the mechanical seal and the rough surfaces previously described when the operating velocity was varied. The friction coefficient f was computed from the total friction torque C_f :

$$f = \frac{2C_f}{(R_o + R_i)F_{\text{closing}}} \tag{18}$$

A decreasing friction zone corresponding to mixed lubrication and an increasing friction zone at higher speeds which is typical of the hydrodynamic regime are observed. It can be seen that for all the tested values of the macro-cells numbers, the Stribeck curves obtained with the multiscale model are correlated with the one computed with the deterministic model. However, a slight difference can be observed in the mixed lubrication regime.



(a) Surface 1



(b) Surface 2

Fig. 7 Comparison of the Stribeck curves obtained with the multiscale and pure deterministic models

The evolution of the cavitation area within the sealing interface is presented in Fig. 8a, b as a function of G . The results obtained with different numbers of macro-cells are presented, as well as the results from the deterministic model. The figures show that the percentage of cavitation increases with the duty parameter G , but the ratio depends on the characteristics of each surface. Generally speaking, the multiscale model tends to underestimate the cavitation fraction compared to the deterministic solution. The error is increased when the number of macro-cells is higher. This is not surprising because at each macro-cell boundary, a constant pressure and thus a full fluid film are imposed,

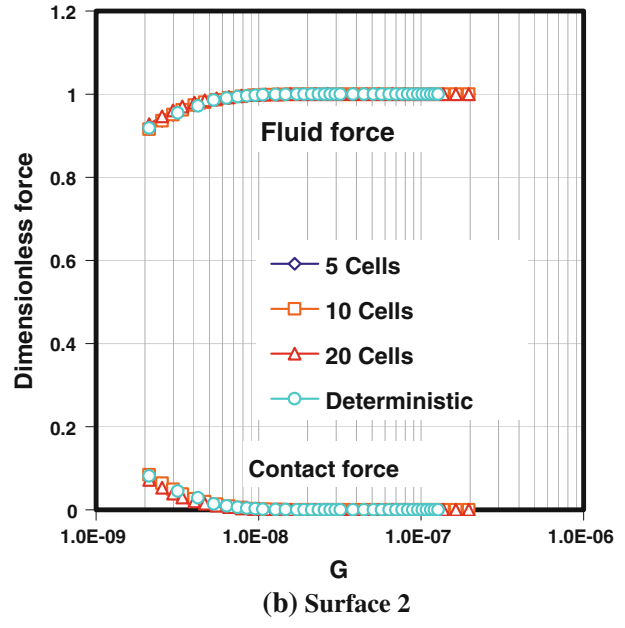
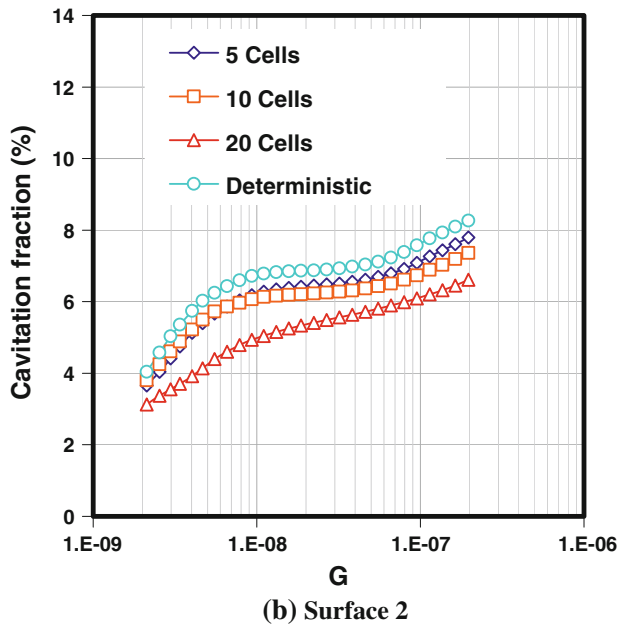
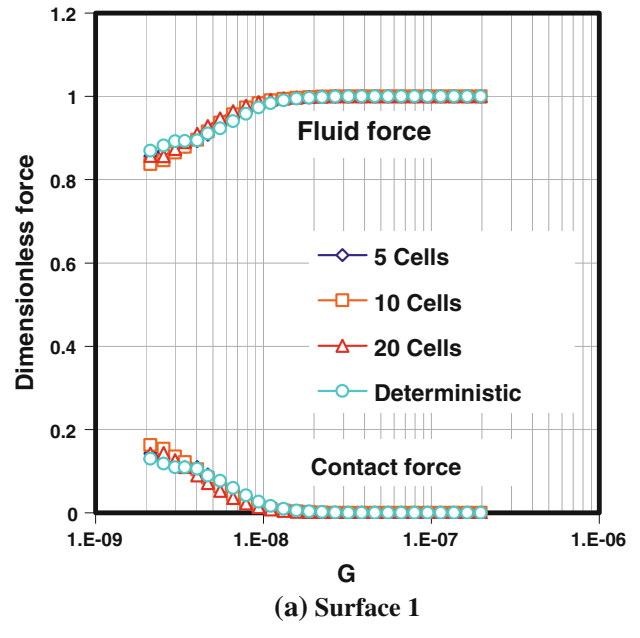
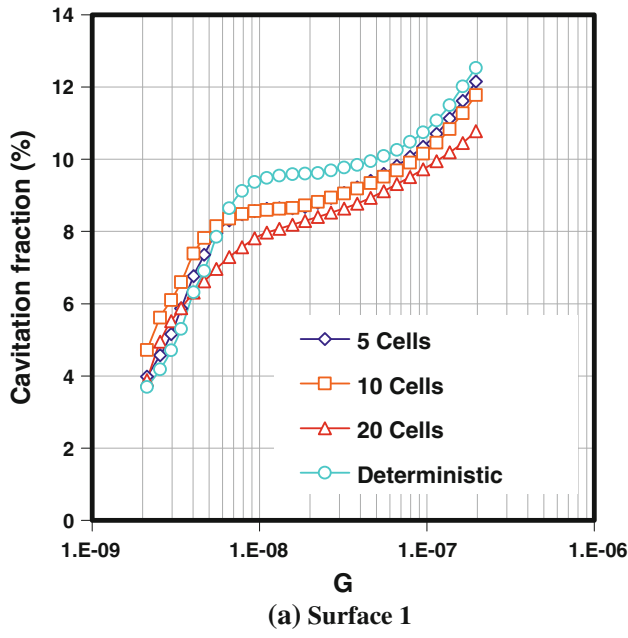


Fig. 8 Cavitation fraction curves obtained with the multiscale and pure deterministic models

Fig. 9 The fluid force and contact force curves obtained with the multiscale and pure deterministic models

whereas a cavitation zone can develop through this boundary in the deterministic solution.

The variations of the hydrodynamic lift and the contact force with the duty parameter G for different numbers of macro-cells are presented in Fig. 9a, b and compared to the deterministic results. It can be observed that the generated hydrodynamic lift increases with the duty parameter. The hydrodynamic effect that contributes to the seal rings separation unloads the asperities in contact. Consequently, the contact force tends to zero when the duty parameter G is increased. The curves obtained with the different

numbers of macro-cells do not perfectly overlap in the mixed lubrication zone before reaching the critical value of G , where the transition to the hydrodynamic lubrication regime takes place and the contact force vanishes. However, the multiscale model exhibits a reasonable agreement with the deterministic approach and can quite accurately define the transition between the lubrication regimes.

Figure 10a, b presents the average distance of separation between the seal rings versus the duty parameter G calculated with the deterministic and the multiscale models. Obviously, the film thickness increases with G because of

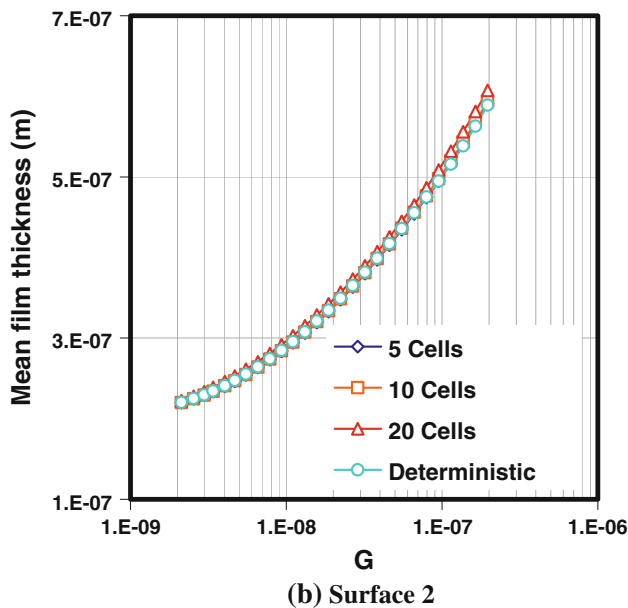
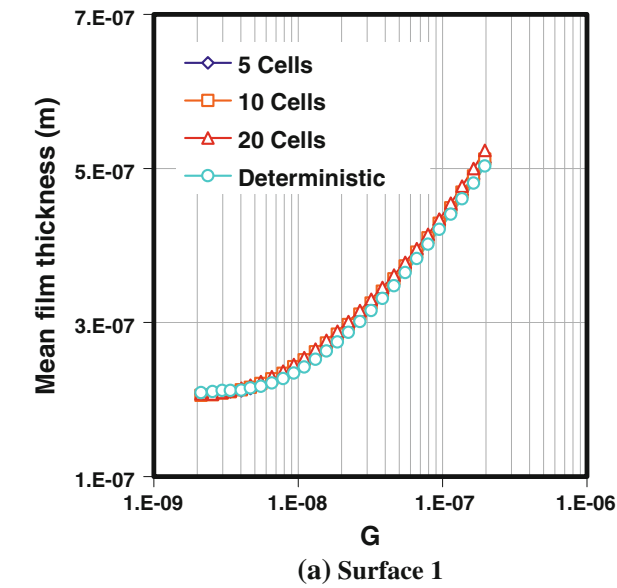


Fig. 10 The film thickness curves obtained with the multiscale and pure deterministic models

the hydrodynamic lift enhancement. The film thickness obtained with surface 1 is thinner than the one corresponding to surface 2. This is correlated with the cavitation fraction (Fig. 8) and the calculated friction (Fig. 7). The results show that the multiscale model leads to an accurate estimation of the film thickness for all the macro-mesh tested here.

4.2 Model Performance

This objective of the present approach is to reduce the computation time compared to a deterministic solution.

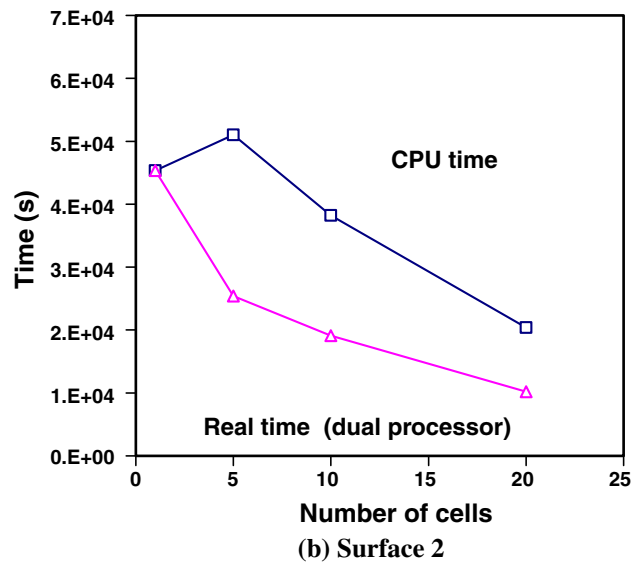
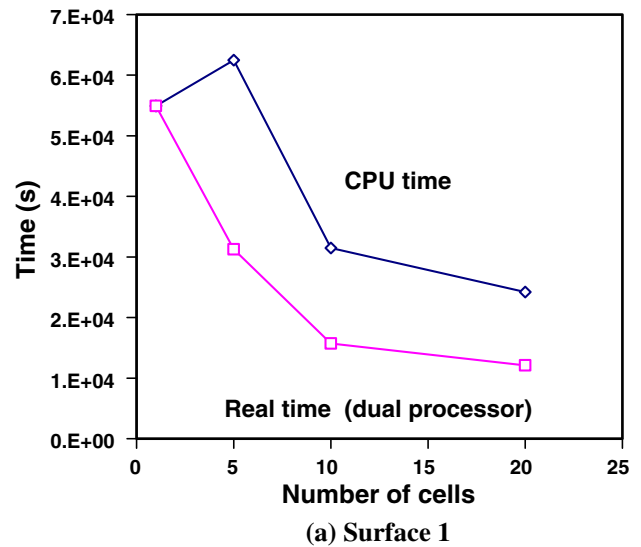
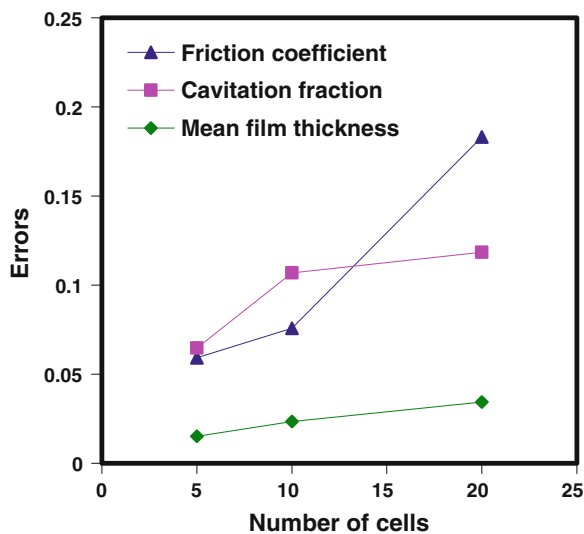
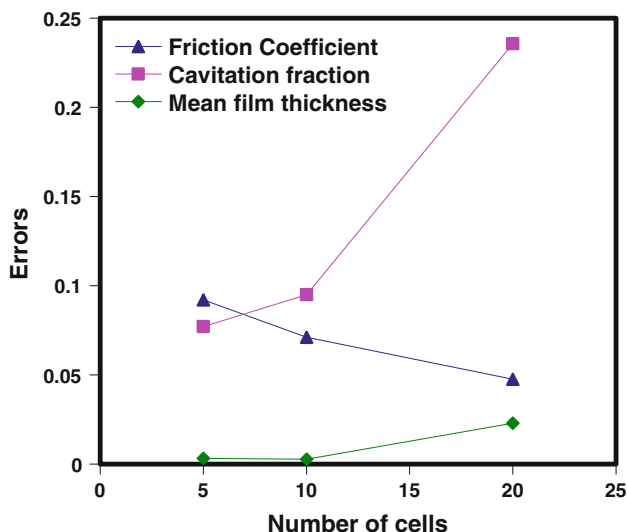


Fig. 11 Computation time for different cell numbers

This is why the microscopic domain was divided into sub-domains. Moreover, from the programming point of view, the multiscale approach presented here offers a very simple and reliable way for parallelization, since the computation on the micro-scale can be performed simultaneously for each macro-cell. Figure 11a, b gives, as a function of the number of macro-cells, the computation time necessary to obtain the entire Stribeck curves previously presented. The first point (i.e. one macro-cell) corresponds to the deterministic simulation. First of all, when the number of macro-cells is higher than five, the total CPU time is significantly reduced compared to the deterministic solution. Secondly, because of the parallel computation, the total computation time is shared between the processor, thus reducing the real computation time. The simulations have been carried out on a dual processor system, which is why



(a) Surface 1



(b) Surface 2

Fig. 12 Errors on the average friction coefficient, cavitation fraction and mean film thickness

Table 3 Data obtained from surface 1

| | Deterministic case | 5 macro-cells | 10 macro-cells | 20 macro-cells |
|----------------------|--------------------|---------------|----------------|----------------|
| Friction coefficient | 2.769E-02 | 2.901E-02 | 2.897E-02 | 2.514E-02 |
| Film thickness (m) | 3.052E-07 | 3.093E-07 | 3.114E-07 | 3.156E-07 |
| Cavitation (%) | 8.958 | 8.609 | 8.715 | 8.060 |

Table 4 Data obtained from surface 2

| | Deterministic case | 5 macro-cells | 10 macro-cells | 20 macro-cells |
|----------------------|--------------------|---------------|----------------|----------------|
| Friction coefficient | 2.020E-02 | 2.098E-02 | 2.117E-02 | 2.030E-02 |
| Film thickness (m) | 3.598E-07 | 3.591E-07 | 3.604E-07 | 3.685E-07 |
| Cavitation (%) | 6.674 | 6.177 | 6.029 | 5.129 |

the real computation time indicated in Fig. 11a, b is approximately divided by two. If a more efficient computer with four or eight processors is used, the real computation time can be more significantly reduced.

However, the decrease in computation time is also followed by a loss in results accuracy. The average relative errors, compared to the deterministic solution, of the friction coefficient, the mean film thickness and the cavitation area are presented in Fig. 12a, b. The results were calculated over the entire duty parameter range previously presented and depend on the characteristics of the surface. Generally speaking, the average error on these parameters increases with the number of macro-cells (except for one marginal case). The error arises from the boundary condition used between the sub-domains, where a constant pressure is imposed. This pressure ensures a global mass conservation but not a local mass conservation. Even if the error on cavitation fraction can reach values as high as 20 %, the error on film thickness is comparatively very small (lower than 5 %). The averaged values used to compute the error are presented in Tables 3 and 4.

4.3 Local Deterministic and Multiscale Comparison

The main simplification used in the multiscale model is to conserve the mass flow globally (from macro-cell to macro-cell), but not locally. This allows a reduction in computation time, but also induces a certain error compared to a pure deterministic solution, as previously discussed. The objective of this section is to observe the local pressure distribution and to analyse the effect of this assumption.

The pressure distribution for the both models with the same operating condition ($G = 2.12E-8$) and surface are plotted in Fig. 13. As previously stated, the simulations are carried out with 4,000 nodes in the radial direction and 200 in the circumferential direction. The macro-mesh is obtained by dividing the total micro-mesh in the radial direction by the number of macro-cells. Here, the simulation was performed with 20 macro-cells.

Fig. 13 Pressure distribution obtained with the deterministic and multiscale models with $N_{bl} = 20$ (surface 1)

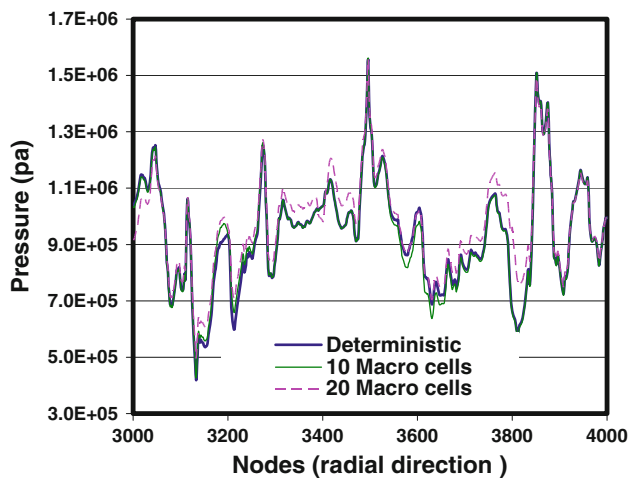
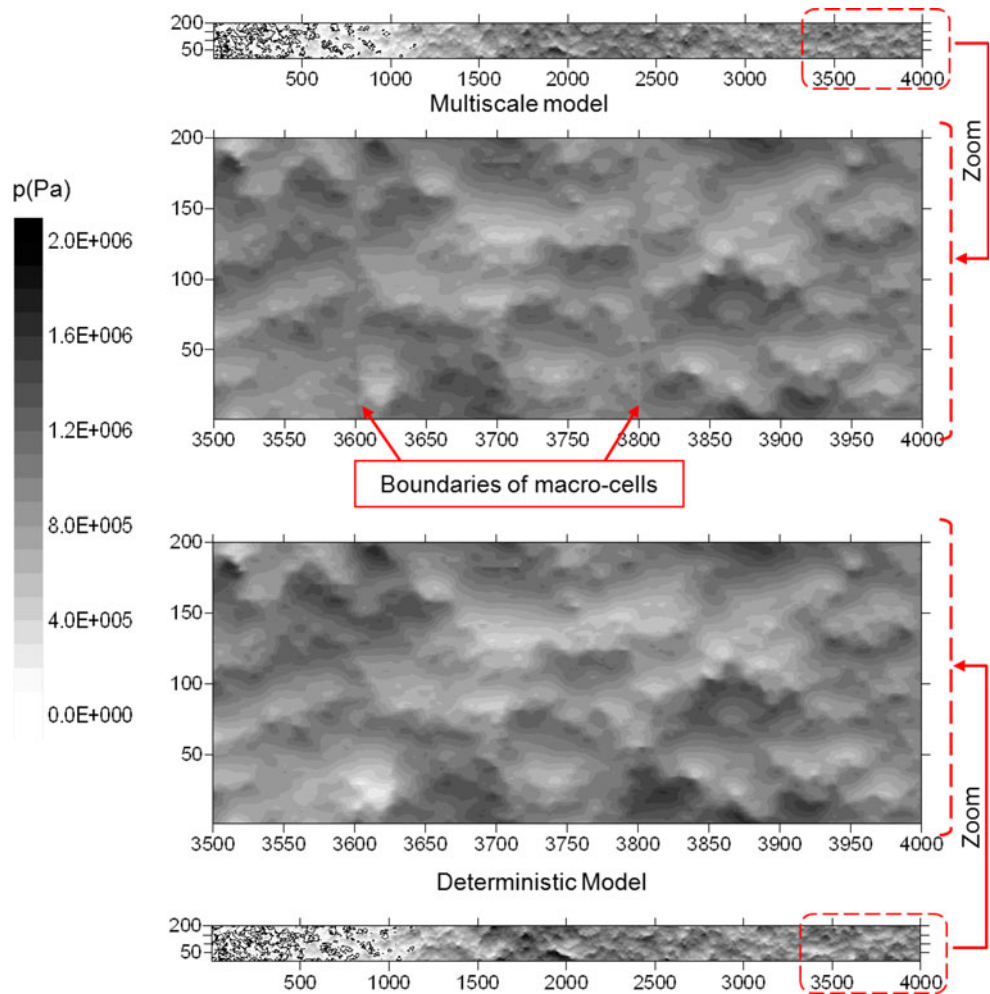


Fig. 14 Pressure profile comparison obtained from deterministic and multiscale model (surface 1)

The pressure fields presented in Fig. 13 indicate a good correlation between the two models. The transition from one macro-cell to another is difficult to detect. For convenience, a part of the figure has been zoomed into show the

way the studied area is subdivided and more clearly see the effect of constant pressure at the boundaries. Moreover, pressure profiles obtained from the deterministic and multiscale simulations are compared in Fig. 14. This shows that even if the multiscale model locally affects the pressure distribution in the vicinity of the macro-cell boundaries (node 3600 and 3200 for 10 and 3800, 3600, 3400 and 3200 for 20 macro-cells), it has a relatively weak effect on the whole local distribution. This illustrative example is developed further to support the multiscale model assumptions.

4.4 Macroscopic Pressure Distribution

Figure 15a, b presents the macroscopic pressure distribution for both surfaces when G is varied. As expected, when G increases, the global level of fluid pressure rises because of the hydrodynamic pressure generation. An interesting point is the following: the leakage flow occurs from the high pressure zone (outer radius) to the low pressure zone (inner radius). However, the macroscopic pressure gradient can be inverted to the general pressure gradient and the resulting leakage flow. This means that a kind a radial fluid pumping must be

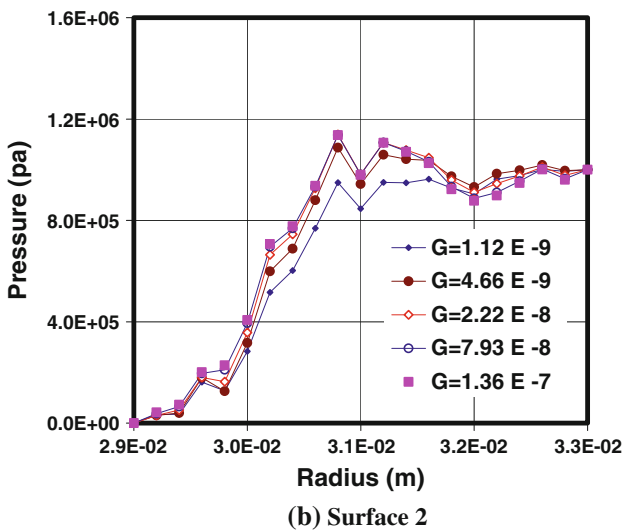
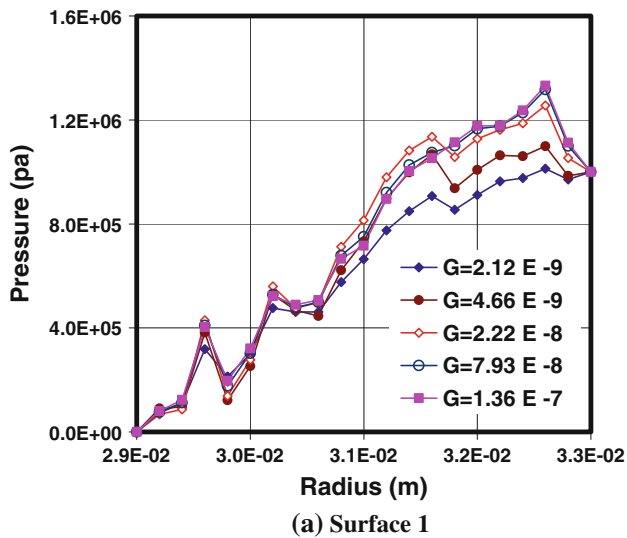


Fig. 15 Evolution of the macroscopic pressure distribution ($N_{bl} = 20$)

generated within each macro-cell when one surface is moving. The amount of pumping is different from one cell to the other, leading to different pressure gradients at the boundaries of the element. This effect is at the origin of the pressure build up which can lead to macroscopic pressure values higher than the feeding pressure and finally to faces separation.

The influence of the number of macro-cells on the macroscopic pressure distribution is illustrated in Fig. 16a, b. A good agreement between the results is obtained even if an increase in the number of sub-domains leads to an increase in the error.

5 Conclusion

A multiscale approach for mixed lubrication has been presented. It is based on a micro-deterministic model

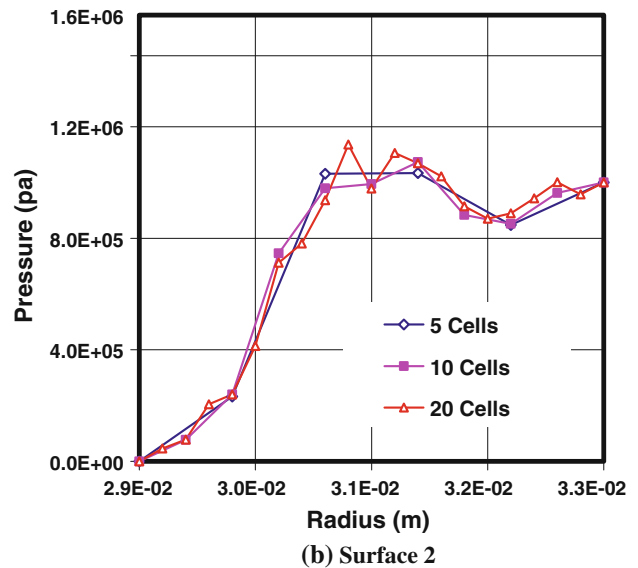
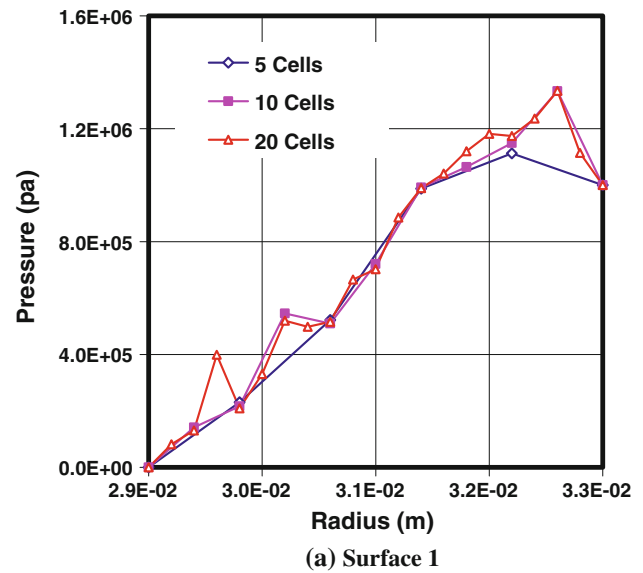


Fig. 16 Influence of the number of macro-cells on the macroscopic pressure distribution ($G = 1.96E-07$)

working on a small area, coupled with a macro-scale model providing the pressure distribution on a macro-mesh.

The results from the multiscale model are correlated with those obtained by a deterministic model. Since the studied area is subdivided into macro-cells, the numerical resolution can be carried out by means of parallel computation. This approach allows a significant reduction of the computation time, while maintaining reasonable accuracy compared to a full deterministic approach. The macroscopic pressure provides comprehensive information explaining the roughness-induced pressure generation, which is not easily obtained with a full deterministic solution.

The presented multiscale approach can be extended to a two-dimensional configuration, in order to deal with large domains.

Acknowledgments The authors acknowledge the “Sealing Technology Department” of CETIM for supporting this research project.

References

1. Lebeck, A.O.: Principles and Design of Mechanical Face Seals. Wiley, New York (1991)
2. Tzeng, S.T., Saibel, E.: Surface roughness effect on slider bearing lubrication. ASLE Trans. **10**, 334–338 (1967)
3. Christensen, H.: Stochastic models for hydrodynamic lubrication of rough surfaces. Proc. IME **184**, 1013–1022 (1970)
4. Patir, N., Cheng, H.S.: An average flow model for determining effects of three-dimensional roughness on partial hydrodynamic lubrication. J. Lubr. Technol. **100**, 12–17 (1978)
5. Patir, N., Cheng, H.S.: Application of average flow model to lubrication between rough sliding surfaces. J. Lubr. Technol. **101**, 220–230 (1979)
6. Evans, H.P., Snidle, R.W.: Analysis of micro-elastohydrodynamic lubrication for engineering contacts. Tribol. Int. **29**(8), 659–667 (1996)
7. Jiang, X., Hua, D., Cheng, H.S., Ai, X., Lee, S.: A mixed elastohydrodynamic lubrication model with asperity contact. J. Tribol. **121**, 481–491 (1999)
8. Zhu, D., Hu, Y.Z.: A full numerical solution to the mixed lubrication in point contact. J. Tribol. **122**, 1–9 (2000)
9. Dobrica, M.B., Fillon, M., Maspeyrot, P.: Mixed elastohydrodynamic lubrication in a partial journal bearing—comparison between deterministic and stochastic models. J. Tribol. **128**(4), 778–788 (2006)
10. Minet, C., Brunetiere, N., Tournerie, B.: A deterministic mixed lubrication model for mechanical seals. J. Tribol. **133**(4), 042203 (2011)
11. Hamilton, D., Walowit, J., Allen, C.: A theory of lubrication by micro-irregularities. J. Basic Eng. **88**, 177–185 (1966)
12. Hou, T.Y., Wu, X.H.: A multiscale finite element method for elliptic problems in composite materials and porous media. J. Comput. Phys. **134**, 169–189 (1997)
13. Jenny, P., Lee, S.H., Tchelepi, H.A.: Multiscale finite volume method for elliptic problems in subsurface flow simulation. J. Comput. Phys. **187**, 47–67 (2003)
14. Hamrock, B.J., Dowson, D.: Ball Bearing Lubrication. Wiley, New York (1981)
15. Minet, C., Brunetière, N., Tournerie, B., Fribourg, D.: Analysis and modelling of the topography of mechanical seal faces. Tribol. Trans. **53**(6), 799–815 (2010)